Carbohydrate Polymers 343 (2024) 122480

Contents lists available at ScienceDirect

Carbohydrate Polymers

journal homepage: www.elsevier.com/locate/carbpol

Chitosan nanocoatings *N*-acylated with decanoic anhydride: Hydrophobic, hygroscopic and structural properties

Péter Márton [a], Adél Rácz [b], Beáta Szolnoki [c], János Madarász [d], Norbert Nagy [b], Bálint Fodor [e], Péter Basa [e], János Rohonczy [f], Zoltán Hórvölgyi [a,*]

[a] Budapest University of Technology and Economics, Faculty of Chemical Technology and Biotechnology, Department of Physical Chemistry and Materials Science, Centre for Colloid Chemistry, H-1111 Budapest, Műegyetem rkp. 3, Hungary
[b] Institute for Technical Physics and Materials Science, Centre for Energy Research, H-1121 Budapest, Konkoly Thege Miklós út 29-33, Hungary
[c] Budapest University of Technology and Economics, Faculty of Chemical Technology and Biotechnology, Department of Organic Chemistry and Technology, H-1111 Budapest, Műegyetem rkp. 3, Hungary
[d] Budapest University of Technology and Economics, Faculty of Chemical Technology and Biotechnology, Department of Inorganic and Analytical Chemistry, H-1111 Budapest, Hungary
[e] Semilab Semiconductor Physics Laboratory Co. Ltd., H-1117, Budapest, Prielle Kornélia utca 2, Hungary
[f] Eötvös Loránd University, Faculty of Science, Institute of Chemistry, Department of Inorganic Chemistry, H-1117 Budapest, Hungary

ARTICLE INFO

Keywords:
Chitosan
Dip-coating
N-acylation
Self-assembled structures
Hydrophobicity
Hygroscopicity

ABSTRACT

Thin (ca. 340 nm) chitosan coatings were deposited onto glass substrates via dip-coating, then modified with the methanol solution of decanoic anhydride (0.17–56 mM). NMR, FTIR and XPS measurements confirmed that the acylation degree increased from 18 % to 45 %, and at the highest degree, the whole layer was acylated homogeneously by the reagent molecules. The coating thickness increased (up to 60 %), and the refractive index decreased (from 1.541 to 1.532) due to the acylation, that was determined by UV–visible spectroscopy. The AFM did not reveal morphological changes, but wetting tests showed that the acylation rendered the coating hydrophobic (water contact angle increased from ca. 75° to 100°). The contact angle, however, decreased to 85° due to the development of a second molecular layer of the decanoic acid by-product at the highest (over 25 mM) reagent concentrations. XRD studies showed a self-assembling structuring of the alkyl-chains in the bulk phase, which occurred in the case of the highest degree of acylation. This also manifested itself in a significant decrease of the layer hygroscopicity: the swelling degree decreased from 40 % to 8 % in a saturated water atmosphere monitored by spectroscopic ellipsometry.

1. Introduction

Surface and bulk polarities of thin polymer layers are of great interests in number of applications: separation processes (Seidi et al., 2022), corrosion protection (Szőke et al., 2019, 2020), controlled drug release (Dabóczi et al., 2016) or sensorics (Xu et al., 2023). Nowadays, the biopolymer films have a great popularity in technologies due to their eco-friendly behaviour (Morin-Crini et al., 2022; Wang, Chen, et al., 2022).

Chitosan is a well-known biopolymer (Sebestyén et al., 2020) that is widely used from the food industry (Mujtaba et al., 2019) to medicine (Rezaei et al., 2021). Due to its free amino groups, it has pH-responsive properties (Gyarmati et al., 2022) and can be functionalized relatively easily. The latter enables the production of hydrophobic chitosan, during which an aliphatic side chain is usually attached to the polymer by an acylation reaction with acid chlorides or acid anhydrides (Jin & Wang, 2022). Long-chain fatty acids are most often used for this purpose (e.g. palmitic- or stearic acid (Xiaodong Wang et al., 2019)), but medium- or shorter-chain carboxylic acids can also be suitable (Choi et al., 2007; Hu et al., 2007). The chitosan derivatives developed in this way can be used in medicine (drug delivery or tissue engineering (Cho et al., 2012) or even in corrosion protection (Shamsheera et al., 2020).

* Corresponding author at: Budapest University of Technology and Economics, Faculty of Chemical Technology and Biotechnology, Department of Physical Chemistry and Materials Science, Centre for Colloid Chemistry, H-1111 Budapest, Műegyetem rkp. 3, Hungary.
E-mail addresses: marton.peter@vbk.bme.hu (P. Márton), racz.adel@ek.hun-ren.hu (A. Rácz), szolnoki.beata@vbk.bme.hu (B. Szolnoki), madarasz.janos@vbk.bme.hu (J. Madarász), nagy.norbert@ek.hun-ren.hu (N. Nagy), balint.fodor@semilab.hu (B. Fodor), peter.basa@semilab.hu (P. Basa), janos.rohonczy@ttk.elte.hu (J. Rohonczy), horvolgyi.zoltan@vbk.bme.hu (Z. Hórvölgyi).

https://doi.org/10.1016/j.carbpol.2024.122480
Received 1 February 2024; Received in revised form 27 June 2024; Accepted 9 July 2024
Available online 10 July 2024

These studies often deal with this system in the form of nanoparticles or hydrogels and rarely as a coating. Hydrophobic chitosan coatings could be produced from chitosan molecules modified in the solution phase (Chen et al., 2013; Niemczyk et al., 2019). Nevertheless, the polymer easily precipitates due to the non-polar side groups in an aqueous medium, causing unwanted difficulties in the preparation. The use of non-polar solvents, however, is not suggested due to the environmental requirements. The post-treatment of the deposited chitosan layer can offer an alternative way (Márton et al., 2020, 2023), but due to the hindered diffusion of large reagent molecules (having long alkyl-chains), uniform modification of the coating in its entire depth is not straightforward. Studies dealing with this modified polymer are relatively rare and not for coatings. Several authors have studied that decanoic acid-grafted chitosan can stabilize oil-in-water Pickering emulsions containing natural oils (Meng et al., 2023; Rajaei et al., 2023; Tabatabaei et al., 2022; Y. Yang et al., 2023), and the porous sponge containing the modified polymer might serve as an ideal hemostatic dressing used in tissue engineering (Wang, Dang, et al., 2022). Chitosan and decanoic acid are natural materials (both are used in the food industry, the former as food supplement and packaging material, and the latter as a flavoring substance (Comission Implementing Regulation (EU), *n.d.*). Furthermore, the decanoic acid-grafted chitosan is biocompatible and biodegradable (Lee et al., 2014), so the modified coating is environmentally friendly.

The aim of this work was to prepare hydrophobic chitosan nanocoatings with a non-hygroscopic bulk character. For this purpose acylation of deposited chitosan layer was carried out with the methanol solution of decanoic anhydride. The *N*-acylation can take place at room temperature, and as we suppose, the relatively long alkyl-chains can effectively form the non-polar character of the layer but are short enough that their molecules penetrate deeply into the layer. We also hypothesize that when the coating dries, the non-polar chains are oriented in the direction of the non-polar air phase, which mask the non-acylated regions, (e.g. the OH-groups). This contributes to increasing the hydrophobicity. Previously, this was not possible with short-chain acetyl groups. Rather, the surface became more hydrophilic through *N*-acetylation of the chitosan coating (Márton et al., 2023) and, interestingly, the permeability against hydrated cations was improved significantly (Márton et al., 2024).

The effect of the modification on the surface was studied by wettability tests and the coating composition across the whole layer thickness was investigated by XPS. The water absorbing studies was carried out by spectroscopic ellipsometry. These types of coatings can serve in corrosion protection as a barrier layer against harmful aqueous solutions and water molecules in a humid environment.

2. Experimental section

2.1. Reagents

All chemicals were used as received without any further purification. Methanol (99.9 % a.r.), isopropanol (99.7 %, f.a.) were provided by Reanal (Hungary), sulfuric acid (96 %, f.a.) by Carlo Erba (Italy), and acetic acid (99.8 % f. a.) by Lachner (Czech Republic). Chitosan (Medium molecular weight: 200,000–300,000 Da, Degree of deacetylation: 75–85 %), decanoic anhydride (96 %, f.a.), diiodomethane (Reagent-Plus®, 99 %, contains copper as stabilizer) and formamide (Reagent-Plus®, 99.0 %,) were purchased from Merck (Germany). Water was purified by an Adrona system (Adrona Integrity+) and had a specific electrical resistance of 18.2 MΩcm (ultrapure water).

2.2. Sample preparation

2.2.1. Coating preparation

Before dip-coating, the glass substrates (soda-lime glass microscope slides, Menzel-Gläser, Germany) were cleaned using 5 % (*w*/w) aqueous detergent solution, 10 % sulfuric acid solution, isopropanol and ultrapure water. The 1 % chitosan solution was made by dissolving 0.5 g chitosan in 49.5 mL 1 % (*v*/v) acetic acid solution (made by mixing 500 μL acetic acid with 49.0 g ultrapure water). The solution was stirred for 24 h, then centrifuged (30 min, 4000 rpm, HERMLE Z36 HK) to remove any insoluble particles. The coating deposition was performed at 25 °C from the chitosan solution with a dip coater made by Plósz Mérnökiroda Kft. (Budapest, Hungary), with 5 cm/min withdrawal speed. After a single dipping, the coatings dried overnight at room temperature.

2.2.2. Chemical modification of the coatings

To produce possibly hydrophobic surfaces, some of the prepared coatings were *N*-acylated in a methanol solution of decanoic anhydride with the method reported by Choi et al. (Choi et al., 2007). The schematic illustration of the reaction is shown in Fig. 1.

50 mL reagent solution was prepared by mixing methanol and the appropriate amount of decanoic anhydride, in which six parallel samples were chemically modified at the same time by shaking at room temperature for 24 h on a laboratory shaker (Heidolph Rotamax 120). After the reaction, the *N*-acylated samples were immersed into 25 mL of pure methanol and shaken for approximately 10 s, then dried in a fume hood at room temperature for 30 min. Eight different reagent concentration of decanoic anhydride was used according to Table 1. The native (not modified) chitosan samples were abbreviated as CS and the *N*-acylated samples as DCSX, where X increases from 1 to 8 with increasing reagent concentrations. Table 1. also shows the molar equivalent value of the amounts of reagents used per unit of glucosamine in each case. This was calculated from the amount of chitosan in each sample based on surface area (25×30 mm on both side of the substrate) and layer thickness (calculated by UV–Visible spectroscopy, see section 2.3).

For ^{13}C solid NMR measurements, 50 mg chitosan powder was acylated with the same method. The powder was grinded, then dispersed in 174 mL methanol with 3540 μL decanoic anhydride, and stirred for 24 h (that way the reagent concentration and molar equivalent value are the same as those used for the acylation of DCS8 coatings). After the reaction, the DCS8 powder was washed with methanol, filtered, and dried at room temperature.

As shown in Fig. 1, the amino groups of the chitosan used to prepare the coatings were partially acetylated (approximately 15–25 % according to the manufacturer). After the reaction, the originally acetylated groups remained acetylated (two-carbon side chains) and additional groups were acylated by the decanoic anhydride (resulting ten-carbon side chains). Hereinafter, the percentage of monomer units containing two-carbon side chains in the polymer is called the degree of acetylation and is denoted by *DA(Acetyl)*. Similarly, the percentage of all acylated amino groups is called the degree of acylation and is denoted by *DA* (the latter therefore includes the percentage of monomer units containing two-carbon and ten-carbon side chains). For the unmodified chitosan *DA* is equal to *DA(Acetyl)*.

2.3. UV–visible spectroscopic studies

To study the optical properties and calculate the thickness of the coatings, the transmittance spectra of the samples were recorded with an Analytik Jena Specord 200 UV–Vis spectrophotometer with a measurement speed of 10 nm/s, in the 350–1100 nm wavelength range with 1 nm resolution to study their optical properties. The thickness and refractive index of the coatings were determined by fitting a thin-layer optical model to the transmittance spectra (Hild method (Hild et al., 2007)) of six replicate samples.

2.4. NMR spectroscopic studies

In order to calculate the exact degree of acetylation (*DA(Acetyl)*) value of the chitosan used for the preparation of the coatings, and the DA value of the acylated DCS8 powder, NMR spectroscopic studies were

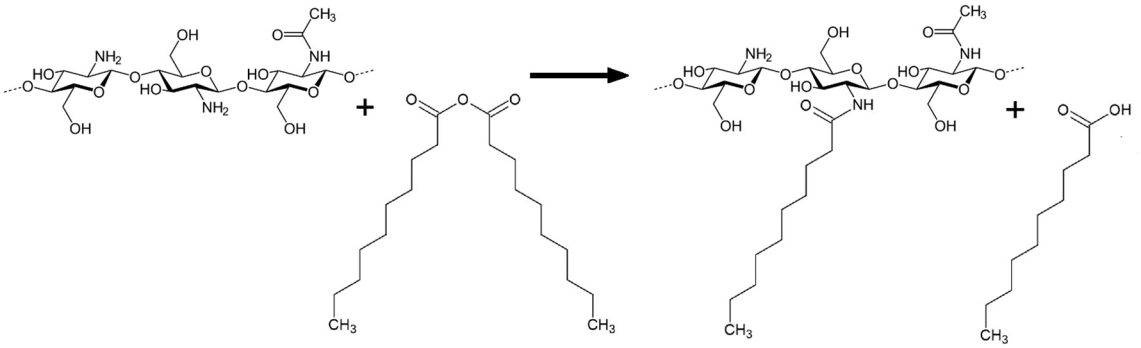

Fig. 1. Modification of the chitosan forming the nanocoating with decanoic anhydride. The reaction produces decanoic acid as a by-product.

Table 1
Concentrations of decanoic anhydride used to modify coatings. In the third column, the amount of the reagent was also given in relation to the amount of glucosamine units of chitosan in the coating.

Sample	Reagent concentration [mM]	Molar equivalent [−]
CS	0	0
DCS1	0.17	0.1
DCS2	0.54	0.3
DCS3	1.57	0.9
DCS4	2.66	1.5
DCS5	7.98	4.5
DCS6	13.57	7.6
DCS7	27.98	15.5
DCS8	55.96	31

performed with the method reported by Heux et al. (Heux et al., 2000). ^{13}C CP-MAS NMR spectra were recorded by Bruker Avance-III 500 MHz NMR spectrometer at 11.744 T using 4 mm BB/1H MAS probe and ZrO rotor. 2048 data points were acquired with 5 s relaxation delay at 125.77 MHz in a 300 ppm wide spectral window. Standard Bruker *cp* cross polarization pulse sequence was used with ramp90100.100 shaped proton CP pulse and 2 ms contact time. After Fourier transformation 8 K spectrum points were applied to get integral *v*alues.

The *DA(Acetyl)* value of the unmodified chitosan material was determined by the integral ratio of the acyl carbon signal (I_{CH3}) at about 25 ppm related to the C1-C6 signals (D-glucopyranosyl ring, I_{C1-6}) in the range of 50 ppm to 120 ppm (Eq. 1) (Kasaai, 2010). The *DA* value of the DCS8 sample were calculated with a similar equation using the carbonyl carbon signals described in the Appendix.

$$DA = \frac{I_{CH_3}}{\frac{1}{6} \bullet \sum I_{C1-6}} \bullet 100\ [\%] \tag{1}$$

2.5. FTIR spectroscopic studies

To study the effect of the reaction on the chemical structure of the coatings, the infrared spectra of the samples were recorded in ATR mode using a Bruker Tensor 37 FT-IR spectrometer, equipped with deuterated triglycine sulfate detector in the 4000–650 cm^{-1} wavenumber range with the resolution of 4 cm^{-1}. The baseline-correction of the spectra was carried out with the OPUS 5.5 software. The *DA* of the coatings was calculated with the method reported by Sabnis and Block from the spectra of six replicate samples using the following equation (Eq. 2) (Sabnis & Block, 1997):

$$DA = 2,33 + \frac{26,486 \bullet A_{1655}}{A_{3445}}\ [\%] \tag{2}$$

where A_{1655} and A_{3445} were the absorbances at 1655 cm^{-1} (vibration peak of the amide group) and 3450 cm^{-1} (vibration peak of the OH group) respectively. In the case of the unmodified coating, *DA* was equal to *DA(Acetyl)*.

2.6. X-ray diffraction measurements

For investigating the structure of polymer layers grazing incidence angle X-ray diffraction (XRD) patterns were collected using an X'pert Pro MPD (PANalytical B.v.) device equipped with X'celerator detector and a Cu K-α radiation source (λ = 1.54 Å), operating at 40 kV and 30 mA. The intensity was recorded in continuous scanning mode at 0.5° of grazing incidence angle in the scattering range of 4–44° with a step size of 0.0167° and 45 s per step.

2.7. Wettability and surface free energy

To characterize the hydrophobicity and chemical composition of the surface and to calculate the surface free energy, wettability measurements were performed. The advancing (Θ_A) and receding (Θ_R) contact angles were measured with water, diiodomethane and formamide. Measurements were carried out with a Drop Shape Analysis System (DSA30, Krűss GmbH) using the sessile drop method and the drop-build-up technique. Advancing contact angles were determined within the first 20 s after the droplet formation using a drop volume of 10 μL at 25 °C and at least 80 % humidity in a closed chamber. Receding contact angles were measured after removing 5 μL liquid from the droplet. The equilibrium contact angle (Young's contact angle, Θ_Y) was estimated using the Wolfram-Faust equation (Eq. 3) (Ábrahám et al., 2020; Wolfram & Faust, 1978):

$$\Theta_Y = cos^{-1}\left(\frac{cos\Theta_A + cos\Theta_R}{2}\right) \tag{3}$$

The total surface free energy values and the surface free energy components were calculated with the LW-AB approach (van Oss model) (Carel J. van Oss et al., 1988). According to this the surface free energy is composed of a so-called Lifshitz–van der Waals component (γ^{LW}) and an acid–base interaction component (γ^{AB}). The latter can be expressed in terms of an electron acceptor and an electron donor component (Eq. 4):

$$\gamma^{AB} = 2\sqrt{\gamma^{+}\gamma^{-}} \tag{4}$$

where γ^{+} is the electron acceptor (Lewis-acidic), and γ^{-} is the electron donor (Lewis-basic) component. In order to calculate the surface free energy components of the solid surface, the contact angle data of three liquid is needed (one of them must be non-polar and the other two should be polar). During the calculation, the values of the contact angles and surface tension components of the individual liquids must be substituted into the following equation given by the model (Eq. 5) (C. J. van Oss, 1993), and then the three components of the surface energy of the solid surface can be determined from the three equations thus obtained (Szafran et al., 2023).

$$\gamma_{LV}(1+cos\Theta_Y) = 2\sqrt{\gamma_{LV}^{LW}\gamma_{SV}^{LW}} + 2\sqrt{\gamma_{LV}^{+}\gamma_{SV}^{-}} + 2\sqrt{\gamma_{LV}^{-}\gamma_{SV}^{+}} \quad (5)$$

where the subscripts S, L and V denote solid, liquid and vapour phases, respectively. The determining component of the surface free energy of a solid surface provides information about the nature of the moieties on the surface (non-polar, Lewis-acidic or Lewis-basic). Surface tension components of the liquids were used from Ref. (Mohammed-Ziegler et al., 2006).

The change in the advancing contact angles of water droplets was also recorded for 10 min after dropping the liquid in order to characterize the stability of the surfaces. The values were calculated from the contact angles of at least four droplets.

2.8. AFM measurements: Surface morphology

In order to examine the surface morphology of the samples, the AFM images were recorded with an AIST-NT SmartSPM 1000 AFM device in tapping mode with a PPP-NCHR-20 needle (nominal radius < 20 nm, made by NanoSensors). The height and phase image of the samples were recorded in a range of 2 × 2 and 20 × 20 μm. The data evaluation was carried out using the Gwyddion software (Index @ Gwyddion.Net, *n.d.*).

2.9. XPS measurements

In order to study the chemical composition of coatings on the surface and in the deeper layers XPS measurements were performed in a Thermo Scientific ESCALAB Xi$^+$ instrument. The spectra were recorded applying Al K α X-ray source (1486.6 eV), the size of the X-ray spot was 900 μm. The samples were measured as received, afterwards MAGCIS™ argon ion source operating in cluster mode (8 keV, cluster size 500, angle of incidence 45° respect to the surface normal) in a 3 mm area was applied for revealing the component in-depth distributions. Charge neutralizer was used in standard electrostatic mode. Survey spectra were measured in steps of 0.5 eV with 10 ms dwell time per data point. Silicon (2p), carbon (1 s), nitrogen (1 s), oxygen (1 s) high-resolution spectra were measured within the spectral range of interest (ca. 20 eV around the core level emission peaks) at 30 eV pass energies with 0.1 eV steps and 50 ms dwell time per data point. The evaluation of the data was performed in CasaXPS software described in detail in the Appendix.

2.10. Ellipsometric measurements

To characterize the hygroscopic properties of the bulk material of coatings, the swelling of native and modified coatings in water vapour was studied by spectroscopic ellipsometric method. The Δ (phase difference between the *p*- and the *s*-polarized reflected light) and Ψ (amplitude ratio) parameters were recorded with a Semilab EP 12 (ellipsometric porosimeter) device as functions of the wavelength in the 300–800 nm range at 60° angle of incidence. The device evacuated the sample chamber, then increased the relative pressure of the water vapour between 0 and 1 in units of 0.1 to study the water sorption of the coatings (waiting 10 min at each step to reach the equilibrium). After recording the points of the sorption sequence, the relative pressure was decreased the same way in 0.1 steps to study the desorption process.

The layer thickness and refractive index of the coatings at each relative pressure were determined on each pressure level by fitting an optical model to the resulting Ψ and Δ spectra with Semilab's Spectroscopic Ellipsometry Analyzer (SEA) software (described in detail in the Appendix). The degree of swelling *(S)* was calculated from the layers thickness values with the following equation (Eq. 6):

$$S = \frac{d - d_{dry}}{d_{dry}} \bullet 100\ [\%] \quad (6)$$

where d_{dry} and d are the layer thickness of the coating in the dry and swollen state respectively.

2.11. Statistical analysis

Mean with standard deviation and ANOVA ($p < 0.05$) test was used to the statistical analysis using OriginPro 8.6 software (OriginLab Corporation, Northampton, MA, USA). Significant differences in the tables and figures are marked with lowercase letters, where the different letters mean significantly different data points (Compact Letter Display). If there are multiple letters above a data point, it means that the given data point is not significantly different from several points, which are, however, significantly different from each other.

3. Results and discussion

3.1. Thickness and refractive index of the coatings: UV–visible spectroscopic measurements

It could be observed with the naked eye that the coatings were contiguous and homogenous before the reaction as well as after. The thickness and refractive index of the coatings were measured with thin layer optical analysis by fitting an optical model to the transmittance spectra. Some typical recorded spectra for the bare glass substrate, CS and two different DCS coatings are shown in Fig. 2a.

The average thickness of the coatings before the *N*-acylation was 340 ± 10 nm. From the thickness after the reaction, the relative increase can be calculated with the following equation (Eq. 7):

$$\Delta d_{rel} = \frac{d - d_0}{d_0} \bullet 100\ [\%] \quad (7)$$

where d_0 and d is the layer thickness before, and after the *N*-acylation. The calculated Δd_{rel} and refractive index values are shown in Fig. 2b. In the case of the first five reagent concentration (DCS1-DCS5) a slight increasing trend can be observed in the Δd_{rel} values, but the difference is not significant (in fact the relative increase in the layer thickness of the CS and DCS1-DCS3 samples are not significantly different from zero).

For the three largest concentration the layer thickness rapidly increases which can be explained by the assumption that only in the case of such high concentrations could a considerable amount of side chains be integrated into the bulk phase of the coatings. Due to the space-filling and hydrogen bond-reducing effect of these side chains, the polymer network expands and the volume (thickness) of the layer increases (Márton et al., 2023).

Fig. 2b also shows that the refractive index of the coatings slightly decreases as the reagent concentration increases, which can be explained by the decrease in the optical density of the expanding polymer web, due to the side chains. The black letters above the data points of the Δd_{rel} values indicate significant differences between the values (same letter above two points means that the values are not significantly different), and the same is true for the red letters above the points of the refractive index values.

3.2. Effect of chemical modification on the acylation degree

To calculate the degree of acetylation (*DA(Acetyl)*) of the chitosan used for the coatings, and the *DA* value for the DCS8 powder, solid state ^{13}C CP-MAS NMR spectra were recorded of the materials (seen Fig. 3a). For the explanation of the peak notations see Ref. (Facchinatto et al., 2020) and (X. Yang & Müller, 2011). From the ratio of the integrals of the C1-C6 peaks (D-glucopyranosyl ring) and CH_3 peak, the *DA(Acetyl)* can be determined with Eq. 1 (for the exact integral values, see Table A1 in Appendix). This value for the native material (and therefore for CS coatings) is 18 %, which correlates well with the value given by the manufacturer. Similarly the *DA* value for the DCS8 powder (and therefore for DCS8 coatings) is 42 %, calculated with the method described in Appendix. The quantitative ratio of the α-CH_2 carbon in the side chain

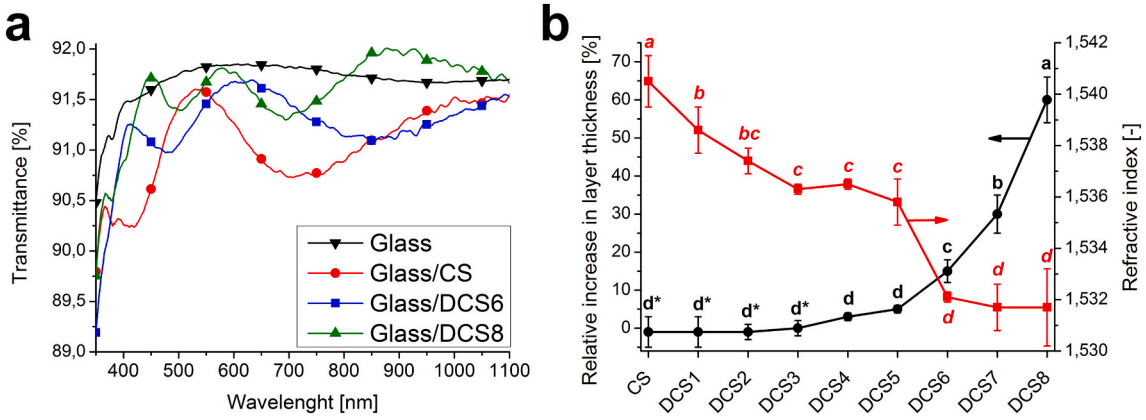

Fig. 2. Typical transmittance spectra for the bare glass substrate, native and some acylated samples (a) and the refractive index and layer thickness changes for samples treated with different concentrations of decanoic anhydride (b). For the abbreviations, see Table 1. The letters above the data points (for the two data lines individually) indicate significant differences: different letters mean significantly different data values in that data line, and the points with asterisk (*) mean that the value is not significantly different from zero. (Mean ± standard deviation, $n = 6$, $p < 0.05$).

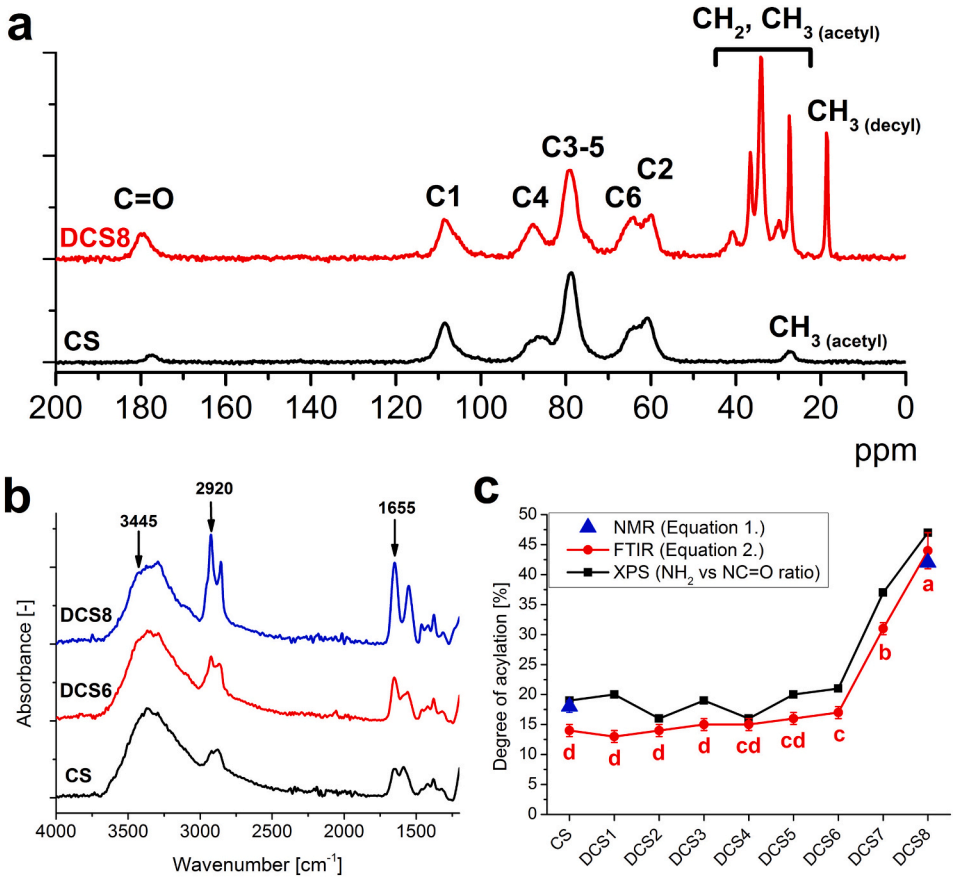

Fig. 3. ^{13}C CP-MAS NMR spectra of the CS and DCS8 powders (a), infrared spectra of the native and two differently *N*-acylated samples (b) (for the peak notations see text) and the degree of acylation calculated from the measurements (c, in the case of NMR, for CS and DCS8 only) (for the abbreviations, see Table 1., the letters below the data points of the values from FTIR measurements indicate the certainty of differences in data values, Mean ± standard deviation, $n = 6$, $p < 0.05$).

and the α-CH_2 carbon in the free acid (by-product) can be determined by decomposing the peaks in the region between 0 and 50 ppm. Based on this, it can be concluded that the ratio of side chains and free acid is 51 % and 49 %, i.e. the by-product remains almost entirely in the coating (probably due to the interactions between the non-polar carbon chains described later in section 3.3). Nie et al. recorded a similar ^{13}CP-MAS NMR spectrum for chitosan modified with lauric acid (12-carbon chain), where the side chains also showed signals in the 0–50 ppm region (Nie et al., 2024).

To study the changes in the chemical composition of the coatings, their FTIR spectra were recorded in ATR mode. Typical spectra are depicted in Fig. 3b for the native and two differently *N*-acylated coating. It can be seen that the intensity of the double peak at the wavenumber of 1655 and 1550 cm^{-1} increases as a result of the reaction. These are called the Amid-I and Amid-II peaks, and they correspond to the the C═O streching vibration, and the N—H bendig vibration of the amide

group, respectively, so that the increase in intensity indicates the completion of *N*-acylation (Atangana et al., 2019; Paula et al., 2020). If the OH groups of the chitosan had also reacted with the decanoic anhydride, the peak of the C═O vibration belonging to the ester group would appear around 1750 cm^{-1}. However, the absence of the peak indicates that only the amino groups were acylated during the reaction (Liu et al., 2013).

Another characteristic peak of the coatings is the double peak around 2920 cm^{-1} (marked in Fig. 3b), which can be associated with the axial deformation of the C—H bonds, and the increase in intensity is due to the increase in the amount of aliphatic side chains integrated into the polymer (Le Tien et al., 2003; Taubner et al., 2020).

Based on the infrared spectra, the degree of acylation (*DA*) can be calculated using Eq. 2 from the intensity ratio of the O—H vibration peak (3445 cm^{-1}) and the Amid-I peak (1655 cm^{-1}). The corresponding peaks were marked in Fig. 3b with black arrows, while the results are in Fig. 3c (red circles).

In addition, the *DA* was also determined based on the XPS measurements, where, after decomposing the nitrogen spectra into three components, the peak area of nitrogen in the NHC═O state was divided by the total area and averaged over the entire depth of the coating (black squares on Fig. 3c). The results obtained from the two measurement methods are reasonably close to each other and agree in their tendency. In addition for the CS and DCS8 sample, the *DA* from the FTIR and XPS measurements also agrees well with the results obtained from NMR spectrum data (blue triangles in Fig. 3c). The red letters below the data points of the values calculated from FTIR measurements are indicating significant differences between those values (common letter corresponds to no significant difference). For the CS sample the *DA* value equals with the *DA(Acetyl)* value since it only has two-carbon side chains.

DA does not increase strongly up to the DCS6 sample, however, in the case of the last two applied concentrations, a rapid increase is observed, which highlights that a very large reagent excess is required for an effective reaction. According to our previous results (Márton et al., 2023), in the case of acetic anhydride, a much smaller amount (4.7 M equivalents, i.e. a concentration of about 8 mM) was sufficient to achieve over 95 % *DA*, so these results are probably due to the large size and lower reactivity of the decanoic anhydride molecule (Peydecastaing et al., 2011).

3.3. Grazing incidence angle X-ray diffraction measurements

The structural changes occurring in the bulk phase of the *N*-acetylated coatings were investigated by X-ray diffraction. The XRD patterns for the different samples are summarized in Fig. 4. All coatings show a broad reflection around $2\theta = 20.7°$, coinciding with the reflection of the "Form II" crystal structure of chitosan, denoted with Miller-indices 110 (Samuels, 1981). In the case of the CS-DCS6 samples, no other diffraction peak can be observed, but in the case of the DCS7 and DCS8 samples, a sharp peak appears around $2\theta = 4°$. This diffraction peak is characteristic of chitosan with aliphatic side chains and is shifted toward smaller angles as the length of the side chain increases (Choi et al., 2007). Many authors agree that this diffraction peak indicates the formation of a stable structure in which the aliphatic side chains are arranged in a comb-like structure roughly perpendicular to the chitosan backbones as a result of a so-called"hydrophobic self-assembly" (Le Tien et al., 2003; Wu et al., 2006). In the case of the DCS samples, this structure could only be formed with the two highest applied reagent concentrations (DCS7 and DCS8), which assumes that only in this case was a sufficient amount of side chains present in the bulk phase. This correlates well with the rapidly increasing value of the degree of acylation (see Fig. 3c) and also with the significantly increased layer thickness values (Fig. 2b).

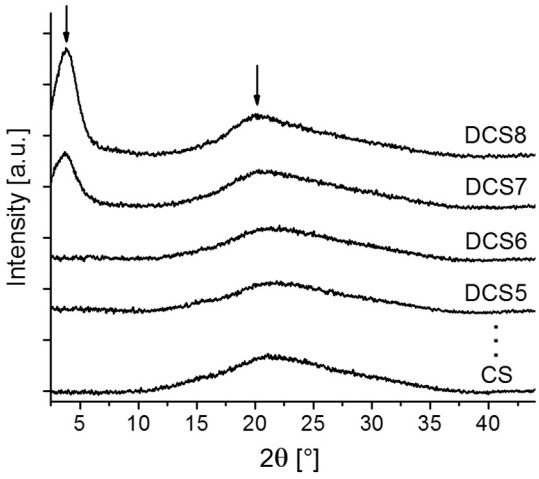

Fig. 4. XRD patterns of the native and differently *N*-acetylated coatings. The diffraction peaks mentioned in the text (around $2\theta = 21°$ characteristic of chitosan, while around $2\theta = 4°$ characteristic of the structure formed by aliphatic side chains) are marked with a black arrows. For the abbreviations, see Table 1, data of samples DCS1-DCS4 are not shown due to the similarity to the DSC5 dataset.

3.4. Wettability and surface free energy of the coatings

To investigate the effect of the *N*-acylation to the wettability and chemical composition of the coatings' surface, the advancing and receding contact angles of water, diiodomethane and formamide were measured on the samples. Since the interaction of surfaces with water is the most important practical parameter, the measured water contact angles are shown in Fig. 5a, while the data for the other two liquids are shown in the Appendix (Fig. A4 and A5). It can be seen that in the case of lower reagent concentrations (up to sample DCS4) the advancing (and receding) contact angles increase rapidly (from ca. 75° to ca. 100°) resulting in a highly hydrophobic surface. However, to further increase the amount of decanoic anhydride, the surface becomes more polar again and the value of the advancing contact angle decreases to around 85°.

From the contact angle data of the three liquids, the surface free energy components of the coating can be calculated by the LW-AB approach (van Oss model) using Eq. 3, 4 and 5 (C. J. van Oss, 1993; Carel J. van Oss et al., 1988). The calculated Lifshitz–van der Waals components (γ^{LW}) and an acid–base interaction components (γ^{AB}) are shown in Fig. 5b, while the electron acceptor (γ^{+}), and the electron donor (γ^{-}) components calculated from the latter one are shown in Fig. 5c for each sample. As can be seen the LW and AB components of the surface energy of the most hydrophobic sample (DCS4) are the smallest and interestingly the electron donor (Lewis-basic) component changes as a curve with minimum.

A possible explanation for the observations is shown in Fig. 5d. When the concentration of decanoic anhydride is low (DCS1-DCS4), the reagent mainly reacts with the free amino groups near the surface of the coating, it does not penetrate deeper into the layer, and the incorporated non-polar side chains migrate to the surface and orientate toward the (non-polar) air phase during the drying (Höhne et al., 2007; Hubbe, 2008). Similar migration and interfacial accumulation of amphiphilic molecules, phosphonated fatty acids incorporated into an acrylic coating were observed by Millet et al. (Millet et al., 2014). This results in the observation that although the layer thickness or the DA of the coatings does not increase significantly (see Fig. 2b and 3b), the composition and structure of the surface layer changes greatly. Hence, non-polar chains appear at the surface (instead of the originally Lewis-basic amino groups), which manifests itself in the decrease of the surface free energy (especially the γ^{-} component) and the increase of the water contact

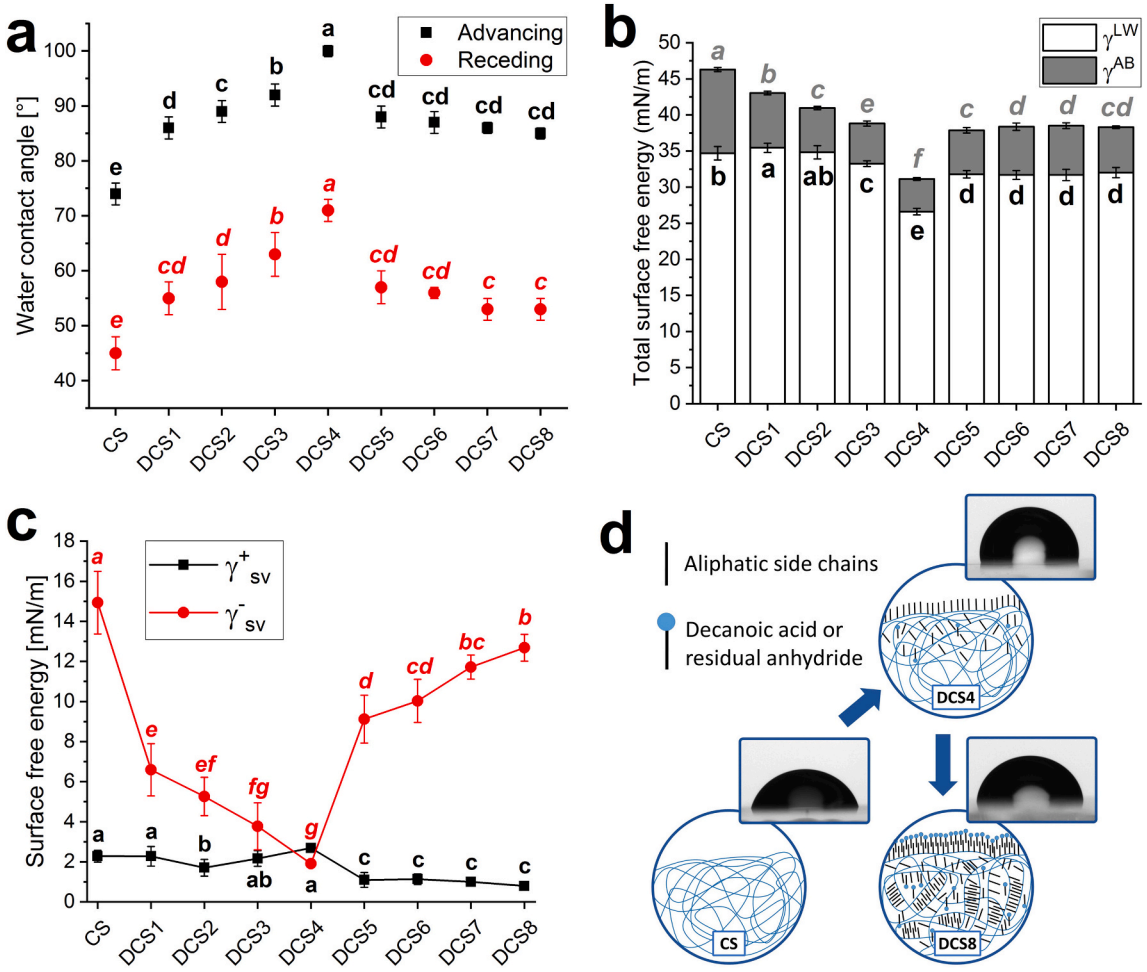

Fig. 5. Water contact angles for CS and all DCS coatings (a), the calculated LW and AB surface free energy components (b), the electron donor and electron acceptor components (c), and a sketch of possible explanation for the results (d). The letters above and next to the data points indicate significant differences: different letters mean significantly different data values. (Mean ± standard deviation, $n = 8$, $p < 0.05$).

angles. Tangpastuhadol et al. have found a similar water contact angle (101 ± 4°) for *N*-stearyl chitosan films, which can be attributed to the layer of non-polar side chains on the surface(Tangpasuthadol et al., 2003).

For higher reagent concentrations (DCS5-DCS8), the surface is completely covered by the aliphatic chains. This can slow down the penetration of decanoic anhydride into the coating, which can explain the observation that the reaction took place significantly only in the case of large reactant excesses (see section 3.2). This ordered structure also enables the formation of a second molecular layer with the opposite

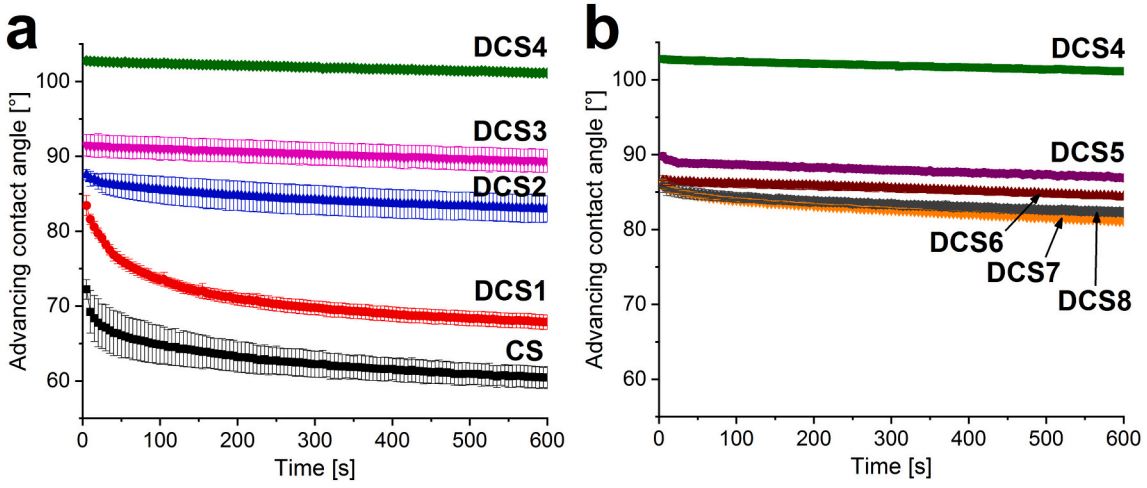

Fig. 6. Time evolution of advancing water contact angles on the surface of the coatings modified with small (a) and large (b) amount of decanoic anhydride. (The data points of the DCS4 sample is shown in both figures for easier comparison, for the abbreviations, see Table 1. Mean ± standard deviation $n = 6$).

orientation on the surface of the coatings from the amphipathic decanoic acid produced in the reaction (Tiberg, 1996; Wooding et al., 1991; Yuan et al., 2007) during the drying of the deposited coating. As a consequence of this, there will be electron donor carbonyl and carboxyl groups at the interface, which results in an increase in the γ^- component (Fig. 5c) and the total surface free energy, and a decrease in water contact angles, as well. The image of the DCS8 sample in Fig. 5d also demonstrates the comb-like structures of the aliphatic chains that appear in the bulk phase, the formation of which is confirmed by X-ray diffraction measurements (see section 3.3).

The temporal stability of the surfaces can be studied by monitoring the time evolution of the advancing water contact angles. The obtained data series are shown in Fig. 6a and b (the data of the DCS4 sample is included in both figures for easier comparison). In the case of the native (CS) coatings, a rapid decrease in the contact angle is observed in the first 50 s of the tests. This is due to the penetration of water molecules into the coating, which promotes the reorientation of functional groups with their polar part toward the water phase (Márton et al., 2024).

As the polarity of the surfaces decreases with increasing amount of reagent, this initial decrease in the value of the contact angles disappears and is no longer observed at all in the case of the DCS4 sample. This is probably due to the extraordinary stability of the ordered structure formed by the aliphatic chains, and the fact that water dropped onto the coating cannot penetrate trough this layer (the slight linear decrease of the contact angles in all samples is probably due to the slow evaporation of the droplet). With the formation of the second surface layer (DCS5-DCS8), a small initial instability can be observed again in the contact angles, which is probably because of an increase in surface polarity.

3.5. Surface morphology of the coatings: AFM studies

In order to study the surface morphology and its possible effect on the wettability, the AFM images of the CS, DCS4 and DCS8 samples were recorded and shown in Fig. 7. The images show the height of the measured surface (the distance perpendicular to the substrate plane). These samples were selected to study the properties of the native, the most hydrophobic and the most *N*-acylated coating.

Although there are visible differences between the height images in both magnification, these are mostly due to the fact that the z-scale magnifies small differences in height, and it can be concluded that the surface of the samples are smooth and reaction does not cause wrinkling, and took place evenly (Márton et al., 2024). The surface roughness factors were 1.002, 1.001 and 1.001 for the CS, DCS4 and DCS8 coatings respectively (determined on 20 × 20 μm^2 areas), which also confirms the smoothness of the surfaces, so the change in wetting characteristics described earlier is caused by differences in chemical composition and not in morphology. The phase images (which characterize the energetic heterogeneity of the surfaces) were completely uniform in all cases (see Fig. A6 in Appendix).

3.6. X-ray photoelectron spectroscopy

In order to investigate the penetration of the decanoic anhydride into the coating, the elemental composition of the samples was examined by X-ray photoelectron spectroscopy. Between each measurement, a thin layer was removed from the surface of the samples with an argon ion source, this way the coatings were examined moving from the surface of the layer toward the substrate. Reaching the substrate was associated with the appearance of the peak of silicon (presented only in glass) in the XPS spectra. The C 1 s and N 1 s peaks were decomposed according to Refs (Maachou et al., 2013) and (Graf et al., 2009) (see Appendix). Assuming that the argon ion source uniformly removes the coating material, and dividing the previously determined layer thickness of the sample by number of etching cycles down to the substrate, the depth position of each measurement can be calculated. Since the acylated material is rich in aliphatic chains, the peak associated with it can provide information about the chemical modification. The proportion of the peak area in relation to the total carbon peak area (C 1 s) is shown in

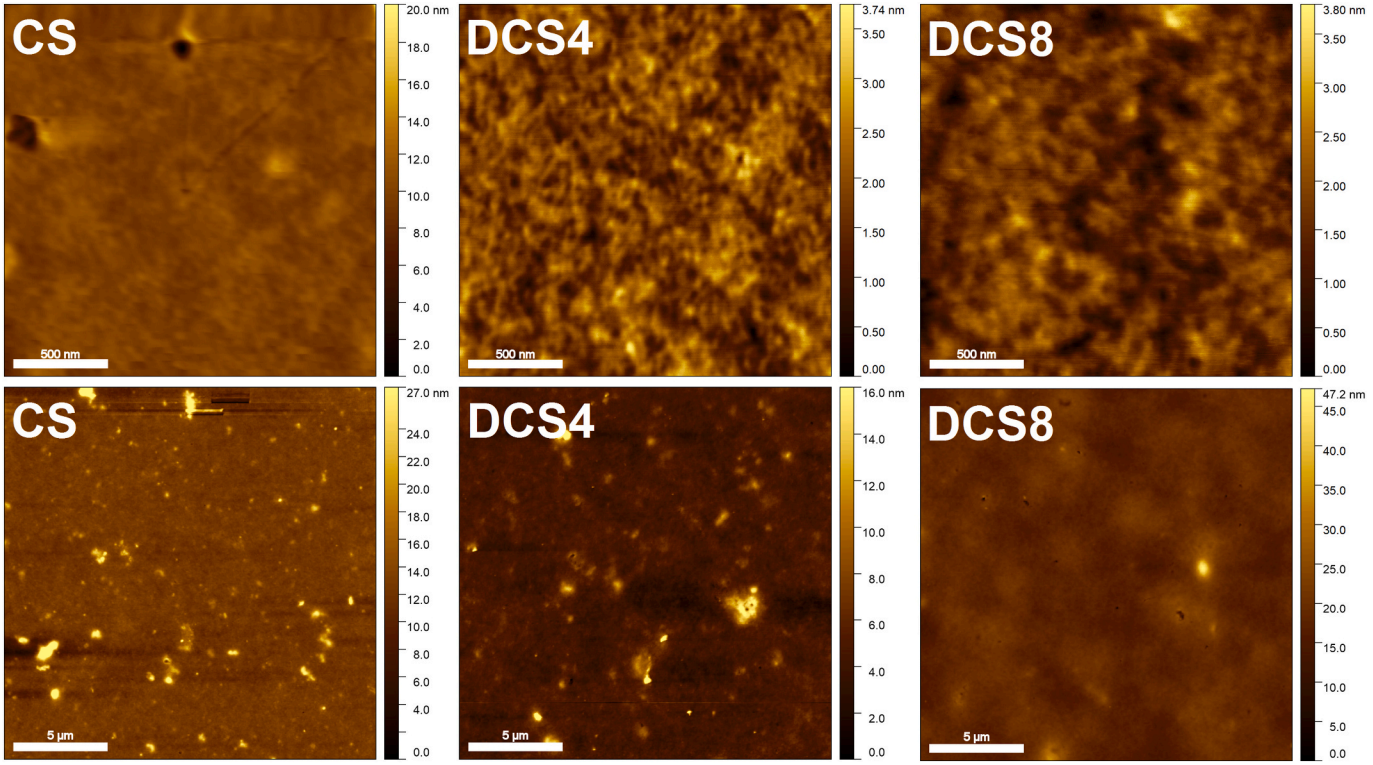

Fig. 7. Height images recorded by AFM on 2 × 2 μm (top) and 20 × 20 μm (bottom) areas for native and two differently *N*-acylated samples. Scale bars are 500 nm (top) and 5 μm (bottom), for the abbreviations, see Table 1.

Fig. 8a and b as a function of the measurement depth (calculated from the surface) for each sample. The data of the DCS4 coating is presented in both figures for easier comparison.

It can be seen from the figure that in all cases up to the DCS6 sample, the ratio of the peak area belonging to aliphatic carbon chains is higher in the surface layer than in the bulk phase. In the case of the native (CS) sample, this is probably due to the surface enrichment of less polar acyl groups, while in the case of the coatings treated with decanoic anhydride, it is due to the aliphatic side chains appearing on the surface. For the DCS7 sample, the reagent penetrated to approximately 60 % of the thickness of the coating, which is shown by the visible step in the peak area ratio (around 300 nm depth) resulted in a *quasi* double-layer structure with an outer carbon-rich hydrophobic and an inner intact layer. In the case of the DCS8 sample, the reaction took place in the entire depth of the coating, the peak ratio belonging to aliphatic chains is uniformly high. The latter two were the concentrations where the DA was large and the additional diffraction peak appeared. Based on these results, the thickness of the acylated layer (green) in relation to the total thickness of the coatings is illustrated in Fig. 8c for the tested samples, which clearly illustrates the effect of different reagent concentrations. This also means, that the thickness ratio of the outer hydrophobic and the inner hygroscopic layer can be finely tuned with the applied reagent concentration, widening the range of applications.

3.7. Swelling in water vapour atmosphere: Spectroscopic ellipsometry studies

In order to determine the behaviour of the modified coatings in a humid environment and the effect of the previously described chemical changes on the degree of swelling, ellipsometric measurements were performed with water vapour in a chamber for the CS, DCS4 and DCS8 samples. The swelling degrees were calculated (using Eq. 6) from the layer thicknesses determined by fitting an optical model to the ellipsometric spectra. The calculated values for the samples are summarized in Fig. 9, where the arrows on the lines indicate the change of the relative pressure (sorption and desorption).

The CS sample gives a sigmoid-shaped, type II isotherm curve, with sorption-desorption hysteresis, which is typical for chitosan and chitosan-based systems (Chalykh et al., 2014; Monte et al., 2018; Tantala et al., 2019). In the case of the DCS4 sample, the swelling degree does not differ significantly from value of the CS coating (since the composition of the bulk phase is practically unchanged, see Fig. 8a and 5d), however, the area of hysteresis loop increases (desorption is less favorable than in the unmodified case). This is probably due to the effect of the hydrophobic surface barrier layer formed from the non-polar carbon chains, which is able to retain water in the polar bulk phase of the coating. For the DCS8 sample, the shape of the isotherm is similar,

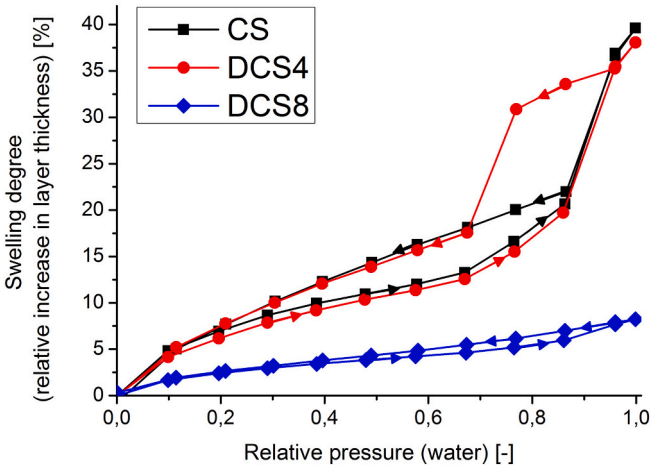

Fig. 9. Calculated swelling degrees at different relative humidity values for the unmodified (CS) most hydrophobic (DCS4) and the most *N*-acylated (DCS8) coatings.

but the maximum swelling degree is significantly lower (ca. 8 % instead of 40 %) and the area of the hysteresis is also smaller. The reason for this is probably that the bulk phase is more hydrophobic due to the presence of a large amount of non-polar side chains and their comb-like structure (*quasi* cross-linking effect), also see Section 3.3 and Fig. 5d.

4. Conclusions

N-acylation of thin chitosan coatings with methanol solution of decanoic anhydride was carried out. The surface and bulk properties of the modified coatings were studied by number of robust techniques like NMR, FTIR, XPS, XRD, AFM, UV–Vis spectroscopy, spectroscopyc ellipsometry and contact angle measurements. The chosen acylating agent made it possible to achieve the goal of experiments: the coating became hydrophobic, while its bulk phase became non-hygroscopic at the highest degree of acylation.

This means that the alkyl chain of the acylating agent was long enough to render the surface hydrophobic, but short enough to allow its molecules to penetrate deeply into the deposited chitosan coatings with a thickness of about 300 nm. According to our assumption, the stability of the chemically modified layers is also based on the fact that self-organized structures were formed as a result of the total acylation. It was also revealed that the lower concentration of the acylating agent resulted in a two layered chitosan film with a non-polar outer and a polar inner part (Fig. 8c). Their relative thickness could be finely tuned

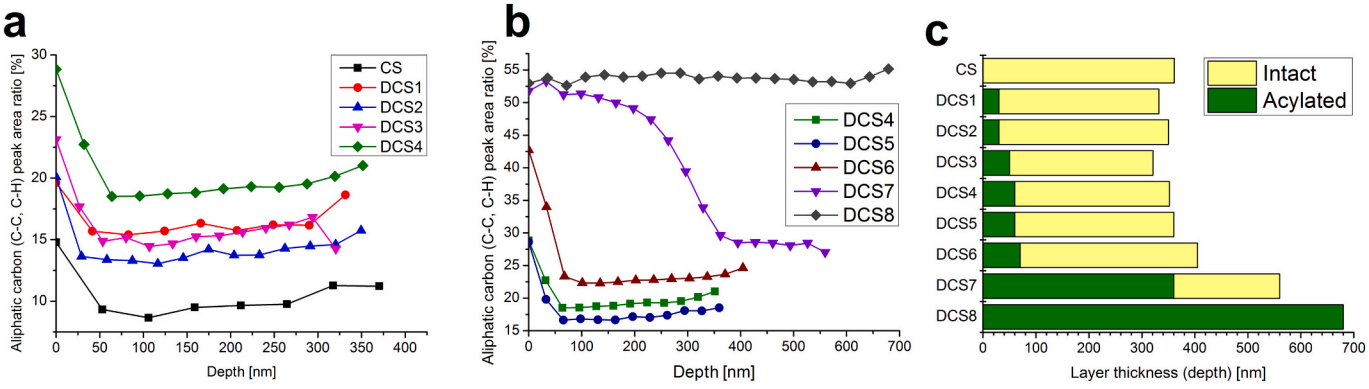

Fig. 8. The peak area ratio of carbon belonging to aliphatic chains in the depth of the sample for the coatings modified with small (a) and large (b) amount of decanoic anhydride (the data points of the DCS4 sample is shown in both figures for easier comparison, for the abbreviations, see Table 1.), and the visualization of the thickness of effectively acylated layer for all the samples (c).

by the concentration of the acylating agent. These types of coatings can serve in corrosion protection as a barrier layer against harmful aqueous solutions and water molecules in a humid environment or for developing water resistance and oleophobic protective layers in food packaging.

CRediT authorship contribution statement

Péter Márton: Writing – original draft, Visualization, Methodology, Investigation, Formal analysis, Conceptualization. **Adél Rácz:** Resources, Methodology, Investigation, Formal analysis. **Beáta Szolnoki:** Resources, Methodology, Investigation, Formal analysis. **János Madarász:** Resources, Methodology, Investigation, Formal analysis. **Norbert Nagy:** Resources, Methodology, Investigation, Formal analysis. **Bálint Fodor:** Resources, Methodology, Investigation, Formal analysis. **Péter Basa:** Resources, Methodology, Investigation, Formal analysis. **János Rohonczy:** Resources, Methodology, Investigation, Formal analysis. **Zoltán Hórvölgyi:** Writing – review & editing, Writing – original draft, Validation, Supervision, Project administration, Methodology, Conceptualization.

Declaration of competing interest

The authors declare that they have no known competing financial interests or personal relationships that could have appeared to influence the work reported in this paper.

Data availability

Data will be made available on request.

Acknowledgments

The authors are thankful to Zsombor Pap for the participation in sample preparation.

Funding

This research was supported by the National Research, Development and Innovation Fund of Hungary [(OTKA) K-128266, (OTKA) FK-128901, Grant TKP2021-NVA-02 and Grant TKP2021-EGA-02].

Appendix A. Supplementary data

Supplementary data to this article can be found online at https://doi.org/10.1016/j.carbpol.2024.122480.

References

Ábrahám, A., Kócs, L., Albert, E., Tegze, B., Szolnoki, B., Nagy, N., Sáfrán, G., Basa, P., & Hórvölgyi, Z. (2020). Durability of microporous hybrid silica coatings: Optical and wetting properties. *Thin Solid Films, 699*(July 2019), Article 137914. https://doi.org/10.1016/j.tsf.2020.137914

Atangana, E., Chiweshe, T. T., & Roberts, H. (2019). Modification of novel chitosan-starch cross-linked derivatives polymers: Synthesis and characterization. *Journal of Polymers and the Environment, 27*(5), 979–995. https://doi.org/10.1007/s10924-019-01407-0

Chalykh, A. E., Petrova, T. F., Khasbiullin, R. R., & Ozerin, A. N. (2014). Water sorption on and water diffusion in chitin and chitosan. *Polymer Science, Series A, 56*(5), 614–622. https://doi.org/10.1134/S0965545X14050034

Chen, C., Tao, S., Qiu, X., Ren, X., & Hu, S. (2013). Long-alkane-chain modified N-phthaloyl chitosan membranes with controlled permeability. *Carbohydrate Polymers, 91*(1), 269–276. https://doi.org/10.1016/j.carbpol.2012.08.042

Cho, Y., Kim, J. T., & Park, H. J. (2012). Size-controlled self-aggregated N-acyl chitosan nanoparticles as a vitamin C carrier. *Carbohydrate Polymers, 88*(3), 1087–1092. https://doi.org/10.1016/j.carbpol.2012.01.074

Choi, C. Y., Kim, S. B., Pak, P. K., Yoo, D. I., & Chung, Y. S. (2007). Effect of N-acylation on structure and properties of chitosan fibers. *Carbohydrate Polymers, 68*(1), 122–127. https://doi.org/10.1016/j.carbpol.2006.07.018

Comission Implementing Regulation (EU) *No 872/2012*. (n.d.). https://eur-lex.europa.eu/legal-content/EN/TXT/?uri=CELEX:32012R0872.

Dabóczi, M., Albert, E., Agócs, E., Kabai-Faix, M., & Hórvölgyi, Z. (2016). Bilayered (silica-chitosan) coatings for studying dye release in aqueous media: The role of chitosan properties. *Carbohydrate Polymers, 136*, 137–145. https://doi.org/10.1016/j.carbpol.2015.09.025

Facchinatto, W. M., Santos, D. M. dos, Fiamingo, A., Bernardes-Filho, R., Campana-Filho, S. P., Azevedo, E. R. de, & Colnago, L. A. (2020). Evaluation of chitosan crystallinity: A high-resolution solid-state NMR spectroscopy approach. Carbohydrate Polymers, 250(August), 116891. doi:https://doi.org/10.1016/j.carbpol.2020.116891.

Graf, N., Yegen, E., Gross, T., Lippitz, A., Weigel, W., Krakert, S., … Unger, W. E. S. (2009). XPS and NEXAFS studies of aliphatic and aromatic amine species on functionalized surfaces. *Surface Science, 603*(18), 2849–2860. https://doi.org/10.1016/j.susc.2009.07.029

Gyarmati, B., Stankovits, G., Szilágyi, B.Á., Galata, D. L., Gordon, P., & Szilágyi, A. (2022). A robust mucin-containing poly (vinyl alcohol) hydrogel model for the in vitro characterization of mucoadhesion of solid dosage forms. *Colloids and Surfaces. B, Biointerfaces, 213*, Article 112406. https://doi.org/10.1016/j.colsurfb.2022.112406

Heux, L., Brugnerotto, J., Desbrières, J., Versali, M. F., & Rinaudo, M. (2000). Solid state NMR for determination of degree of acetylation of chitin and chitosan. *Biomacromolecules, 1*(4), 746–751. https://doi.org/10.1021/bm000070y

Hild, E., Deák, A., Naszályi, L., Sepsi, Ö., Ábrahám, N., & Hórvölgyi, Z. (2007). Use of the optical admittance function and its WKB approximation to simulate and evaluate transmittance spectra of graded-index colloidal films. *Journal of Optics A: Pure and Applied Optics, 9*(10), 920–930. https://doi.org/10.1088/1464-4258/9/10/023

Höhne, S., Frenzel, R., Heppe, A., & Simon, F. (2007). Hydrophobic chitosan microparticles: Heterogeneous phase reaction of chitosan with hydrophobic carbonyl reagents. *Biomacromolecules, 8*(7), 2051–2058. https://doi.org/10.1021/bm0702354

Hu, Y., Du, Y., Yang, J., Tang, Y., Li, J., & Wang, X. (2007). Self-aggregation and antibacterial activity of N-acylated chitosan. *Polymer, 48*(11), 3098–3106. https://doi.org/10.1016/j.polymer.2007.03.063

Hubbe, M. A. (2008). What is the real value of chitosan's surface energy? *Biomacromolecules, 9*(2), 610–614. https://doi.org/10.1021/bm701199g

Index @ Gwyddion.Net. (n.d.). http://gwyddion.net/.

Jin, H., & Wang, Z. (2022). Advances in alkylated chitosan and its applications for hemostasis. *Macromol, 2*(3), 346–360. https://doi.org/10.3390/macromol2030022

Kasaai, M. R. (2010). Determination of the degree of N-acetylation for chitin and chitosan by various NMR spectroscopy techniques: A review. *Carbohydrate Polymers, 79*(4), 801–810. https://doi.org/10.1016/j.carbpol.2009.10.051

Le Tien, C., Lacroix, M., Ispas-Szabo, P., & Mateescu, M. A. (2003). N-acylated chitosan: Hydrophobic matrices for controlled drug release. *Journal of Controlled Release, 93*(1), 1–13. https://doi.org/10.1016/S0168-3659(03)00327-4

Lee, C., Choi, J. S., Kim, I., Byeon, H. J., Kim, T. H., Oh, K. T., … Youn, Y. S. (2014). Decanoic acid-modified glycol chitosan hydrogels containing tightly adsorbed palmityl-acylated exendin-4 as a long-acting sustained-release anti-diabetic system. *Acta Biomaterialia, 10*(2), 812–820. https://doi.org/10.1016/j.actbio.2013.10.009

Liu, L., Zhou, S., Wang, B., Xu, F., & Sun, R. (2013). Homogeneous acetylation of chitosan in ionic liquids. *Journal of Applied Polymer Science, 129*(1), 28–35. https://doi.org/10.1002/app.38701

Maachou, H., Genet, M. J., Aliouche, D., Dupont-Gillain, C. C., & Rouxhet, P. G. (2013). XPS analysis of chitosan-hydroxyapatite biomaterials: From elements to compounds. *Surface and Interface Analysis, 45*(7), 1088–1097. https://doi.org/10.1002/sia.5229

Márton, P., Albert, E., Nagy, N., Tegze, B., Szabó, G. S., & Hórvölgyi, Z. (2020). Chemically modified chitosan coatings: Wetting and electrochemical studies. *Studia Universitatis Babes-Bolyai, Chemia, 65*(3), 63–79. https://doi.org/10.24193/subbchem.2020.3.05

Márton, P., Nagy, Ö. T., Kovács, D., Szolnoki, B., Madarász, J., Nagy, N., … Hórvölgyi, Z. (2023). Barrier behaviour of partially N -acetylated chitosan layers in aqueous media. *International Journal of Biological Macromolecules, 232*, Article 123336. https://doi.org/10.1016/j.ijbiomac.2023.123336

Márton, P., Szolnoki, B., Nagy, N., Deák, A., Zámbó, D., Szabó, G. S., & Hórvölgyi, Z. (2024). Wetting and swelling behaviour of N-acetylated thin chitosan coatings in aqueous media. *Heliyon, 10*(1), Article e23201. https://doi.org/10.1016/j.heliyon.2023.e23201

Meng, W., Sun, H., Mu, T., & Garcia-Vaquero, M. (2023). Chitosan-based Pickering emulsion: A comprehensive review on their stabilizers, bioavailability, applications and regulations. *Carbohydrate Polymers, 304*(December 2022), Article 120491. https://doi.org/10.1016/j.carbpol.2022.120491

Millet, F., Auvergne, R., Caillol, S., David, G., Manseri, A., & Pébère, N. (2014). Improvement of corrosion protection of steel by incorporation of a new phosphonated fatty acid in a phosphorus-containing polymer coating obtained by UV curing. *Progress in Organic Coatings, 77*(2), 285–291. https://doi.org/10.1016/j.porgcoat.2013.10.002

Mohammed-Ziegler, I., Hórvölgyi, Z., Tóth, A., Forsling, W., & Holmgren, A. (2006). Wettability and spectroscopic characterization of silylated wood samples. *Polymers for Advanced Technologies, 17*, 932–939. https://doi.org/10.1002/pat

Monte, M. L., Moreno, M. L., Senna, J., Arrieche, L. S., & Pinto, L. A. A. (2018). Moisture sorption isotherms of chitosan-glycerol films: Thermodynamic properties and microstructure. *Food Bioscience, 22*(February), 170–177. https://doi.org/10.1016/j.fbio.2018.02.004

Morin-Crini, N., Lichtfouse, E., Fourmentin, M., Ribeiro, A. R. L., Noutsopoulos, C., Mapelli, F., … Crini, G. (2022). Removal of emerging contaminants from wastewater using advanced treatments. A review. In *, Vol. 20, Issue 2. Environmental chemistry letters*. Springer International Publishing. https://doi.org/10.1007/s10311-021-01379-5.

Mujtaba, M., Morsi, R. E., Kerch, G., Elsabee, M. Z., Kaya, M., Labidi, J., & Khawar, K. M. (2019). Current advancements in chitosan-based film production for food technology; A review. *International Journal of Biological Macromolecules, 121*, 889–904. https://doi.org/10.1016/j.ijbiomac.2018.10.109

Nie, C.-Z., Li, Y., Huang, X.-H., Wang, H.-P., Wang, X.-S., Dong, X.-P., Zhu, B.-W., & Qin, L. (2024). Multi-scenario application of chitosan emulsions as fat replacers: Based on the regulation of chitosan hydrophobicity and emulsion rheological properties. *Food Hydrocolloids, 155*(May), Article 110237. https://doi.org/10.1016/j.foodhyd.2024.110237

Niemczyk, A., Goszczyńska, A., Gołda-Cępa, M., Kotarba, A., Sobolewski, P., & El Fray, M. (2019). Biofunctional catheter coatings based on chitosan-fatty acids derivatives. *Carbohydrate Polymers, 225*(June). https://doi.org/10.1016/j.carbpol.2019.115263

van Oss, C. J. (1993). Acid-base interfacial interactions in aqueous media. *Colloids and Surfaces A: Physicochemical and Engineering Aspects, 78*(C), 1–49. https://doi.org/10.1016/0927-7757(93)80308-2

van Oss, C. J., Chaudhury, M. K., & Good, R. J. (1988). Interfacial Lifshitz—Van der Waals and polar interactions in macroscopic systems. *Chemical Reviews, 88*(6), 927–941. https://doi.org/10.1021/cr00088a006

Paula, H. C. B., Silva, R. B. C., Santos, C. M., Dantas, F. D. S., de Paula, R. C. M., de Lima, L. R. M., … Dias, F. G. B. (2020). Eco-friendly synthesis of an alkyl chitosan derivative. *International Journal of Biological Macromolecules, 163*, 1591–1598. https://doi.org/10.1016/j.ijbiomac.2020.08.058

Peydecastaing, J., Vaca-Garcia, C., & Borredon, E. (2011). Bi-acylation of cellulose: Determining the relative reactivities of the acetyl and fatty-acyl moieties. *Cellulose, 18*(4), 1015–1021. https://doi.org/10.1007/s10570-011-9528-9

Rajaei, A., Salarbashi, D., Tafaghodi, M., Sabeti, Z., Sabbagh, F., Rakhshani, S., … Fahmideh-Rad, E. (2023). Evaluation of antimicrobial and structural properties of thyme essential oil-loaded chitosan-Capric acid and chitosan-stearic acid Nanogels. *Journal of Food Quality and Hazards Control, 10*(3), 153–162. https://doi.org/10.18502/jfqhc.10.3.13646

Rezaei, F. S., Sharifianjazi, F., Esmaeilkhanian, A., & Salehi, E. (2021). Chitosan films and scaffolds for regenerative medicine applications: A review. *Carbohydrate Polymers, 273*(September), Article 118631. https://doi.org/10.1016/j.carbpol.2021.118631

Sabnis, S., & Block, L. H. (1997). Improved infrared spectroscopic method for the analysis of degree of N-deacetylation of chitosan. *Polymer Bulletin, 39*(1), 67–71. https://doi.org/10.1366/0003702971938911

Samuels, R. J. (1981). Solid state characterization of the structure of chitosan films. *Journal of polymer science. Part A-2, polymer. Physics, 19*(7), 1081–1105. https://doi.org/10.1002/pol.1981.180190706

Sebestyén, Z., Jakab, E., Domán, A., Bokrossy, P., Bertóti, I., & Madarász, J. (2020). Thermal degradation of crab shell biomass , a nitrogen - containing carbon precursor. Journal of Thermal Analysis and Calorimetry, 142(1), 97–117. doi:https://doi.org/10.1007/s10973-020-09438-9.

Seidi, F., Arabi Shamsabadi, A., Ebadi Amooghin, A., Saeb, M. R., Xiao, H., Jin, Y., & Rezakazemi, M. (2022). Biopolymer-based membranes from polysaccharides for CO2 separation: A review. In , *Vol. 20, Issue 2. Environmental chemistry letters*. Springer International Publishing. https://doi.org/10.1007/s10311-021-01349-x.

Shamsheera, K., Prasad, A. R., & PK, J., & Joseph, A.. (2020). Development of self-assembled monolayer of stearic acid grafted chitosan on mild steel and inhibition of corrosion in hydrochloric acid. *Chemical Data Collections, 28*, Article 100402. https://doi.org/10.1016/j.cdc.2020.100402

Szafran, K., Jurak, M., Mroczka, R., & Wiącek, A. E. (2023). Preparation and surface characterization of chitosan-based coatings for PET materials. *Molecules, 28*(5), 2375. https://doi.org/10.3390/molecules28052375

Szőke, Á. F., Szabó, G. S., Hórvölgyi, Z., Albert, E., Gaina, L., & Muresan, L. M. (2019). Eco-friendly indigo carmine-loaded chitosan coatings for improved anti-corrosion protection of zinc substrates. *Carbohydrate Polymers, 215*, 63–72. https://doi.org/10.1016/j.carbpol.2019.03.077

Szőke, Á. F., Szabó, G. S., Hórvölgyi, Z., Albert, E., Végh, A. G., Zimányi, L., & Muresan, L. M. (2020). Accumulation of 2-Acetylamino-5-mercapto-1,3,4-thiadiazole in chitosan coatings for improved anticorrosive effect on zinc. *International Journal of Biological Macromolecules, 142*, 423–431. https://doi.org/10.1016/j.ijbiomac.2019.09.114

Tabatabaei, M., Ebrahimi, B., Rajaei, A., Movahednejad, M. H., Rastegari, H., Taghavi, E., … Lam, S. S. (2022). Producing submicron chitosan-stabilized oil Pickering emulsion powder by an electrostatic collector-equipped spray dryer. *Carbohydrate Polymers, 294*(April), Article 119791. https://doi.org/10.1016/j.carbpol.2022.119791

Tangpasuthadol, V., Pongchaisirikul, N., & Hoven, V. P. (2003). Surface modification of chitosan films. Effects of hydrophobicity on protein adsorption. *Carbohydrate Research, 338*(9), 937–942. https://doi.org/10.1016/S0008-6215(03)00038-7

Tantala, J., Rachtanapun, C., Tongdeesoontorn, W., Jantanasakulwong, K., & Rachtanapun, P. (2019). Moisture sorption isotherms and prediction models of Carboxymethyl chitosan films from different sources with various plasticizers. *Advances in Materials Science and Engineering, 2019*. https://doi.org/10.1155/2019/4082439

Taubner, T., Marounek, M., & Synytsya, A. (2020). Preparation and characterization of hydrophobic and hydrophilic amidated derivatives of carboxymethyl chitosan and carboxymethyl β-glucan. *International Journal of Biological Macromolecules, 163*, 1433–1443. https://doi.org/10.1016/j.ijbiomac.2020.07.257

Tiberg, F. (1996). Physical characterization of non-ionic surfactant layers adsorbed at hydrophilic and hydrophobic solid surfaces by time-resolved ellipsometry. *Journal of the Chemical Society, Faraday Transactions, 92*(4), 531–538. https://doi.org/10.1039/ft9969200531

Wang, Q., Chen, W., Zhu, W., McClements, D. J., Liu, X., & Liu, F. (2022). A review of multilayer and composite films and coatings for active biodegradable packaging. *npj Science of Food, 6*(1). https://doi.org/10.1038/s41538-022-00132-8

Wang, X., Zhao, H., Cao, Y., Su, Y., Hui, H., & Shen, J. (2019). Surface free energy and microstructure dependent environmental stability of sol–gel SiO2 antireflective coatings: Effect of combined vapor phase surface treatment. *Journal of Colloid and Interface Science, 555*, 124–131. https://doi.org/10.1016/j.jcis.2019.07.056

Wang, X., Dang, Q., Liu, C., Chang, G., Song, H., Xu, Q., … Cha, D. (2022). Antibacterial porous sponge fabricated with capric acid-grafted chitosan and oxidized dextran as a novel hemostatic dressing. *Carbohydrate Polymers, 277*(October 2021), Article 118782. https://doi.org/10.1016/j.carbpol.2021.118782

Wolfram, E., & Faust, R. (1978). *Liquid drops on a tilted plate.* Contact Angle Hysteresis and the Young Contact Angle: In Wetting, Spreading and Adhesion. Academic Press.

Wooding, A., Kilner, M., & Lambrick, D. B. (1991). Studies of the double surfactant layer stabilization of water-based magnetic fluids. *Journal of Colloid and Interface Science, 144*(1), 236–242. https://doi.org/10.1016/0021-9797(91)90254-6

Wu, Y., Seo, T., Sasaki, T., Irie, S., & Sakurai, K. (2006). Layered structures of hydrophobically modified chitosan derivatives. *Carbohydrate Polymers, 63*(4), 493–499. https://doi.org/10.1016/j.carbpol.2005.10.010

Xu, S., de Souza Barbosa, P. H., & Wu, W. (2023). Biopolymers-based skin-interfaced triboelectric sensors. *Nano Research, 16*(9), 11753–11782. https://doi.org/10.1007/s12274-023-5784-x

Yang, X., & Müller, K. (2011). The guest ordering and dynamics in urea inclusion compounds studied by solid-state 1H and 13C MAS NMR spectroscopy. Journal of Molecular Structure, 1006(1–3), 113–120. doi:https://doi.org/10.1016/j.molstruc.2011.08.056.

Yang, Y., Gupta, V. K., Amiri, H., Pan, J., Aghbashlo, M., Tabatabaei, M., & Rajaei, A. (2023). Recent developments in improving the emulsifying properties of chitosan. *International Journal of Biological Macromolecules, 239*(November 2022), Article 124210. https://doi.org/10.1016/j.ijbiomac.2023.124210

Yuan, B., Xing, L. L., Zhang, Y. D., Lu, Y., Mai, Z. H., & Li, M. (2007). Self-assembly of highly oriented lamellar nanoparticle-phospholipid nanocomposites on solid surfaces. *Journal of the American Chemical Society, 129*(37), 11332–11333. https://doi.org/10.1021/ja074235n